Detonation development from a hot spot in methane/air mixtures: effects of kinetic models

Jingyi Su[1], Peng Dai[2], Zheng Chen[1*]

[1] SKLTCS, CAPT, BIC-ESAT, Department of Mechanics and Engineering Science, College of Engineering, Peking University, Beijing 100871, China

[2] Department of Mechanics and Aerospace Engineering, Southern University of Science and Technology, Shenzhen 518055, China

Abstract

Natural gas is a promising alternative fuel which can be used in internal combustion engines to achieve low carbon emission and high thermal efficiency. However, at high compression ratio, super knock due to detonation development might occur. In this study, the autoignitive reaction front propagation and detonation development from a hot spot was investigated numerically and the main component of natural gas, methane, was considered. The objective is to assess the performance of different kinetic models in terms of predicting hot spot induced detonation development in methane/air mixtures. First, simulations for the constant-volume homogeneous ignition in a stoichiometric methane/air mixture was conducted. The ignition delay time, excitation time, critical temperature gradient, thermal sensitivity and reduced activation energy predicted by different kinetic models were obtained and compared. It was found that there are notable discrepancies among the predictions by different kinetic models. Then, hundreds of one-dimensional simulations were conducted for detonation development from a hot spot in a stoichiometric CH_4/air mixture. Different autoignition modes were identified and the detonation regimes were derived based on the peak pressure and reaction front propagation speed. It was found that even at the same conditions, different propagation modes can be predicted by different kinetic models. The broadest detonation development regime was predicted by the reduced GRI mechanism, while a relatively narrow regime was predicted by the recent kinetic model FFCM-1 and Aramco 3.0. The present results indicate that super knock prediction strongly depends on the kinetic model used in simulations. Therefore, significant efforts should be devoted to the development and validation of kinetic models for natural gas at engine conditions.

Keywords: Detonation development; autoignition; hot spot; methane; kinetic model

* Corresponding author. E-mail: cz@pku.edu.cn, Tel: 86-10-62766232.

1. Introduction

Natural gas is a promising alternative fuel which can be used in internal combustion engines (ICEs) to achieve low emission of carbon dioxide and particulate matter.[1] Moreover, spark ignition engines (SIEs) using natural gas can run at relatively high compression ratio or elevated boost pressures to achieve high thermal efficiency. However, the compression ratio in SIEs is constrained by engine knock which can cause severe damage.[2] Recently, the so-called super-knock with pressure oscillation above 200 atm has been identified.[3-9] Such high pressure in super-knock was attributed to detonation development. Therefore, there were many studies[10-26] on detonation development from a hot spot under engine-relevant conditions. However, these studies mainly focused on hydrogen, syngas, or large hydrocarbon fuels while natural gas received little attention. Consequently, there is still incomplete understanding of detonation development from a hot spot in natural gas/air mixtures under engine-relevant conditions. For example, the critical conditions for detonation development were not fully investigated before for natural gas. In this study, the detonation development from a hot spot was studied numerically for methane, which is the main component of natural gas.

The detonation development from a hot spot can be explained by the reactivity gradient theory of Zeldovich[27] and the SWACER (Shock Wave Amplification by Coherent Energy Release) mechanism proposed by Lee et al.[28]. A hot spot can induce an autoignitive reaction front which propagates at the speed u_a. If u_a is close to the local sound speed, a, chemical reaction and pressure wave can couple together which may induce detonation development.[12, 29] To quantify the detonation development regime, Gu et al.[11] proposed a detonation peninsula based on the following two non-dimensional parameters:

$$\xi = \frac{dT_0}{dr} \Big/ \left(\frac{dT_0}{dr} \right)_c \quad , \qquad \varepsilon = \frac{r_0 / a}{\tau_e} \tag{1}$$

where dT_0/dr and r_0 are respectively the temperature gradient and radius of the hot spot with a linear temperature distribution; $(dT_0/dr)_c$ is the critical temperature gradient at which $a = u_a$[11]; and τ_e is the excitation time. Therefore, ξ and ε represent the normalized temperature gradient and the ratio of acoustic time to excitation time, respectively. According to Zeldovich[27], the propagation speed of the hot spot-induced autoignition front is equal to the inverse of the gradient of the ignition delay time τ_i

$$u_a = \left(\frac{d\tau_i}{dr}\right)^{-1} = \left(\frac{d\tau_i}{dT_0}\cdot\frac{dT_0}{dr}\right)^{-1} \tag{2}$$

According to the requirement of $a = u_a$, the critical temperature gradient is[11]

$$\left(\frac{dT_0}{dr}\right)_c = -\left(a\frac{d\tau_i}{dT_0}\right)^{-1} \tag{3}$$

Equations (1)-(3) indicates that the normalized temperature gradient is equal to the ratio of the local sound speed to the autoignitive reaction front propagation speed, i.e., $\xi = a/u_a$.

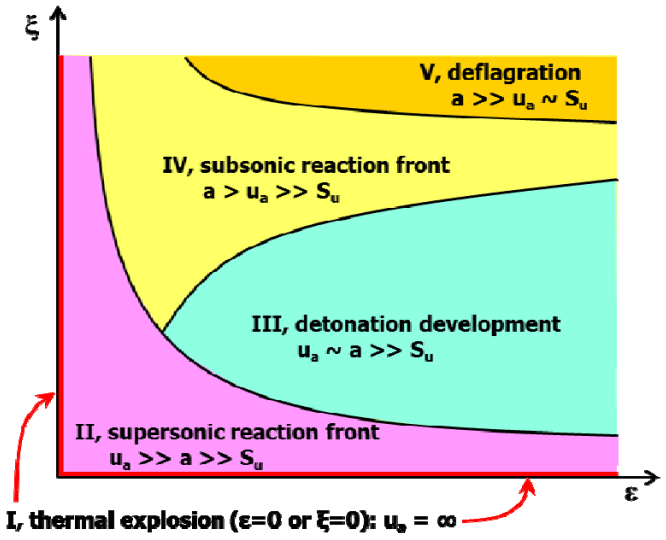

Fig. 1 Schematics of different regimes of autoignitive reaction front propagation induced by a hot spot (figure from Ref. 30). Five modes, I~V, are determined based on the comparison among difference characteristic speeds.

The plot of ξ versus ε in Fig. 1 shows that different modes of autoignitive reaction front

propagation can be classified based on the comparison among the reaction front propagation speed, u_a, the sound speed, a, and the laminar flame speed, S_u[11, 30]. Detonation development occurs in region III in Figure 1. The detonation development regime was used by Bradley and coworkers[14, 15] and Rudloff et al.[16] to quantify the critical conditions for the super-knock phenomenon in SIEs. The detonation development regime was computed for hydrogen[22, 30], syngas[11], methanol[22], dimethyl ether[17, 31, 32], n-heptane[10, 17, 21, 23, 31], iso-octane[10] and toluene reference fuel[19, 20, 22]. However, the detonation development regime for methane was not reported before except the recent work of Pan et al.[22]. Therefore, in this study the detonation development regime was obtained for methane.

Recently, Libermann and coworkers[33, 34] have shown that the prediction of hot spot induced detonation development strongly depends on the kinetic model used in simulations and that simplified one-step or two-step chemical model cannot quantitatively reproduce the autoignitive reaction front propagation from a hot spot. In the literature, there are many kinetic models developed for methane or C_1-C_4 fundamental fuels. It is not clear whether different kinetic models can predict similar detonation development regimes for methane.

Based on the above considerations, this study aims to identify the detonation development regime for methane and to assess the performance of different kinetic models. One-dimensional transient simulations considering detailed chemistry and transport were conducted. In the following sections, the numerical model and methods was briefly introduced first. Then, different modes of autoignitive reaction front propagation and detonation development regime were computed. The performance of different kinetic models was compared against each other. Finally, the conclusions were presented.

2. Numerical model and methods

We considered autoignitive reaction front propagating in a stoichiometric CH_4/air mixture

inside a closed spherical chamber. The hot spot lies in the center of the chamber and it is represented by the following temperature distribution:

$$T(t=0,r)=\begin{cases} T_0+(r-r_0)\dfrac{dT_0}{dr} & \text{for} \quad 0\le r\le r_0 \\ T_0 & \text{for} \quad r_0\le r\le R_w \end{cases} \tag{4}$$

where T_0 is the initial uniform temperature outside the hot spot, dT_0/dr the initial temperature gradient specified inside the hot spot, and r_0 the hot spot radius. The spherical chamber radius was fixed to be R_w = 4 cm. The computational domain was initially filled with a static, stoichiometric CH_4/air mixture with uniformly distributed initial pressure of P_0 = 40 atm. The initial temperature outside the hot spot was fixed to be T_0 = 1300 K.

The in-house code A-SURF (Adaptive Simulation of Unsteady Reactive Flow)[35-37] was used to simulate the one-dimensional transient autoignitive reaction front propagation induced by a hot spot in a spherical coordinate. The conservation equations for multi-component reactive compressible flow were solved using the finite volume method. A-SURF has been successfully used in previous studies on ignition, flame propagation and detonation[38-43]. The details on the governing equations, numerical scheme and code validation for A-SURF can be found in Refs.[35-37] and were provided in the Supplementary Document. It is noted that the real gas effect cannot be considered in our code and the ideal gas equation of state was used in simulation. Very high pressure above 300 atm appeared in our simulation results and thereby the real gas effect needs to be considered in future studies. Nevertheless, the maximum pressure before detonation development is within 100 atm, at which the real gas effect on the calculation of the ignition delay time is within 5% according to Karimi et al. [53]. Therefore, it is expected that the real gas effect on the critical conditions for detonation development is weak. In order to accurately and efficiently resolve the autoignitive reaction front propagation, a multiple level adaptive mesh refining method was adopted. The reaction zone was always covered by

the finest mesh whose size is 2 μm and corresponding time-step is 0.4 ns. Grid convergence was achieved to ensure numerical accuracy (see Fig. S3 in the Supplementary Document). Similar to previous studies, adiabatic, non-penetrative, reflective boundary conditions were used for both boundaries at $r = 0$ and $r = R_w$.

3. Results and discussion

In the literature there are several kinetic models developed for methane or C_1-C_4 foundation fuels. These models are listed in table 1. It is noted that the model, GRI Reduced, was the reduced version of the original GRI Mech. 3.0. These kinetic models were used to calculate the ignition delay time τ_i and excitation time τ_e in a constant-volume homogeneous ignition system. The ignition delay time was defined as the time for the occurrence of maximum temperature rise rate; and the excitation time was defined as the duration between 20% of the maximum heat release rate. The results for a stoichiometric CH_4/air mixture are shown in Table 1 and Fig. 2.

Table 1 Different kinetic models for CH_4 oxidation and the values of critical temperature gradient, $(dT/dr)_c$, ignition delay time, τ_i, and excitation time, τ_e, and for stoichiometric /air at $T_0 = 1300$ K and $P_0 = 40$ atm. *Ns* and *Nr* respectively denote the number of species and reactions.

Mechanism	*Ns*	*Nr*	$(dT/dr)_c$ (K/mm)	τ_i (ms)	τ_e (μs)
FFCM-1[44]	38	291	0.208	0.598	1.30
UCSD Mech.[45]	58	270	0.498	0.352	1.35
Aramco Mech. 3.0[46]	106	800	0.130	0.922	1.08
GRI Mech. 3.0[47]	53	325	0.407	0.330	1.50
GRI Reduced[48]	19	15	0.409	0.328	1.49
DTU Mech.[49]	68	631	0.232	0.639	1.15
HP Mech.[50, 51]	92	615	0.256	0.571	0.95
USC Mech. II[52]	111	784	0.239	0.557	1.42

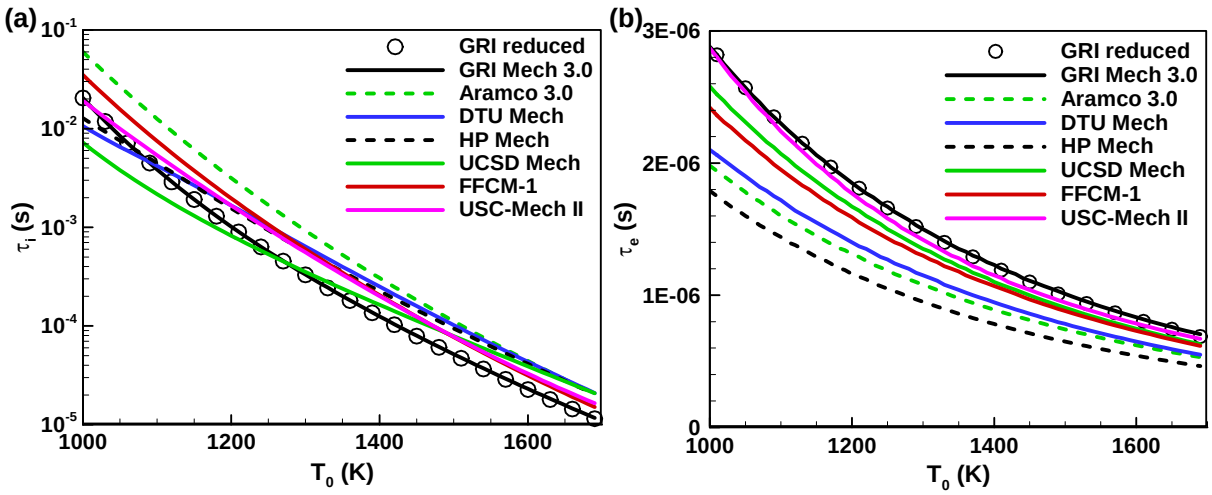

Fig. 2 Change of the (a) ignition delay time τ_i and (b) excitation time τ_e with the initial temperature for stoichiometric CH_4/air at P_0 = 40 atm.

Table 1 and Fig. 2(a) show that there are notable discrepancies among the predictions by different kinetic models. For the initial temperature around 1000 K, the ignition delay time predicted by UCSD Mech. is about one-order smaller than that by Aramco 3.0. The maximum relative difference in τ_i predicted by different kinetic models reduces to 180% for T_0 = 1300 K, which is still notable. Similar observation was reported by the recent study of Karimi et al.[53]. Usually the ignition delay time at high temperature is measured in shock tubes for CH_4/O_2 diluted with argon. To the authors' best knowledge, there is no experimental date for stoichiometric CH_4/air at a broad range of temperature of $900<T_0<1600$ K. Therefore, in Fig. 2(a) we cannot include the experimental data for CH_4/air. For the excitation time, Fig. 2(b) shows that it is in the order of micro-second. The discrepancies in τ_e predicted by different kinetic models are much smaller than those in τ_i. Nevertheless, the maximum relative difference in τ_e is still about 58% for T_0 = 1300 K according to the data in listed in table 1.

Figure 3 shows the critical temperature gradient $(dT/dr)_c$, thermal sensitivity β[33] and reduced activation energy $\overline{E}$[10], which are defined in Eqs. (3) and (5):

$$\beta = -\frac{T}{\tau_i}\frac{\partial \tau_i}{\partial T}, \quad \bar{E} = \frac{\tau_i}{\tau_e}\frac{E}{RT} \tag{5}$$

where E is the global activation energy and R is the universal gas constant. The thermal sensitivity of ignition delay time, β, represents the normalized activation energy.[34] When the ignition delay time is approximated as $\tau_i = A\exp(E/RT)$, we have $\beta = E/RT$, indicating that is the effective global activation energy[33] and it determines the detonation stability. The lower reduced activation energy $\bar{E}$ reflects the stronger coupling of reaction zone with the pressure wave.[10]

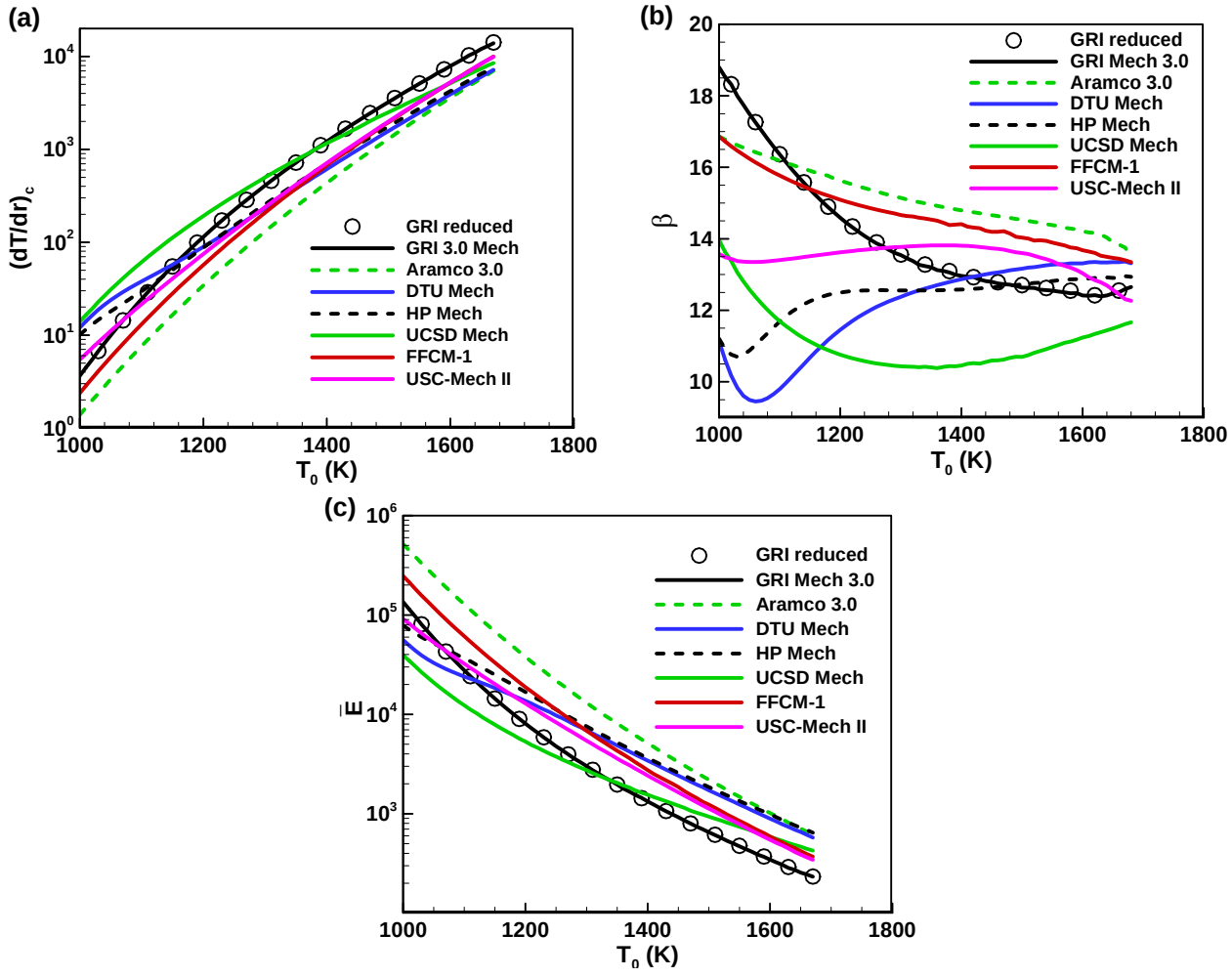

Fig. 3 Change of the (a) critical temperature gradient $(dT/dr)_c$, (b) thermal sensitivity β and (c) reduced activation energy $\bar{E}$ with the initial temperature for stoichiometric CH_4/air at $P_0 = 40$ atm.

Similar to Fig. 2, Fig. 3 also shows notable discrepancies among the predictions by different kinetic models. Figure 3(a) shows that the critical temperature gradient increases with temperature.

According to the data in Table 1, the maximum relative difference in $(\mathrm{d}T/\mathrm{d}r)_c$ predicted by different kinetic models is 151% for T_0 = 1300 K. Figure 3(b) shows that different trends are predicted by these mechanisms. Specifically, monotonic decrease of β with T_0 is predicted by GRI Mech. 3.0 and its reduced version, Aramco 3.0, and FFCM-1; while non-monotonic change is predicted by other kinetic models. As mentioned before, the thermal sensitivity is $\beta = E/RT$, where E is the effective global activation energy E. For GRI Mech. 3.0, Aramco 3.0 and FFCM-1, the effective global activation energy E is not sensitive to the temperature for $1000 < T_0 < 1500$ K and thereby β decreases with T_0. However, for DTU Mech., the effective global activation temperature, E/R, increases faster than the temperature for certain temperature range, and thereby non-monotonic change of β with T_0 is observed. The interpretation on the change of the effective global activation energy with temperature predicted by different kinetic models requires analysis on the reaction path way and the rates of elementary reactions, which is beyond the scope of the current work.

Figure 3(c) shows that $\bar{E}$ always reduces monotonically with T_0. Therefore, the higher the initial temperature, the stronger the coupling between the reaction zone and shock wave and thereby the easier the detonation development. At T_0 = 1300 K, the maximum relative difference in $\bar{E}$ predicted by different kinetic models is 477%. Reduced GRI mechanism has the minimum $\bar{E}$ at T_0 = 1300 K, which may contribute to an easier detonation development. Therefore, different detonation development regime may be predicted by different kinetic models for the same hot spot and initial conditions.

Figures 2 and 3 show that the eight kinetic models listed in table 1 have different predictions of the ignition and excitation time, critical temperature gradient, thermal sensitivity, and reduced activation energy. These values were from 0D simulations of the homogeneous ignition process. For 1D simulations, the boundaries of the detonation development regime were obtained through

trial-and-error; and each line on the detonation development regime required more than one hundred combinations of hot spot radius and temperature gradient. Therefore, even for 1D simulations the computational cost is very large and we only considered three typical kinetic models, GRI Mech., Aramco 3.0 and FFCM-1. GRI Mech. 3.0 and Aramco 3.0 are both popularly used by the combustion community and thereby they were selected here. FFCM-1 was chosen since it can accurately predict the recent experimental data on the ignition delay time (see Figs. 6 and 16 in work of Karimi et al. [53]) and the laminar flame speed (see Fig. 10 in work of Movaghar et al. [54]). Since Figs. 2 and 3 show that the original and reduced GRI Mech. have nearly the same predictions, the reduced version of GRI Mech. was used in 1D simulations to reduce the computational cost.

Hundreds of 1D simulations were conducted for detonation development from a hot spot in a stoichiometric CH_4/air mixture. Figure 4 shows a typical detonation development process predicted by the reduced GRI mechanism for $\xi = 2.8$. It is noted that the values of ξ and ε were calculated based on the states at $r = r_0$. Initially the autoignition front propagates outwardly at the speed in the order of 1000 m/s (lines #2~#5 in Fig. 4). A leading weak shock wave is developed (line #5) and it induces the development of the over-driven detonation (line #6). Since the detonation propagation speed is much larger than the shock speed, the leading shock is caught up and merges with the detonation (line #7). During the detonation propagation, autoignition occurs in the unburned mixture on the right side and eventually thermal run-away happens (line #10). Similar observation was reported before for other fuels.[17]

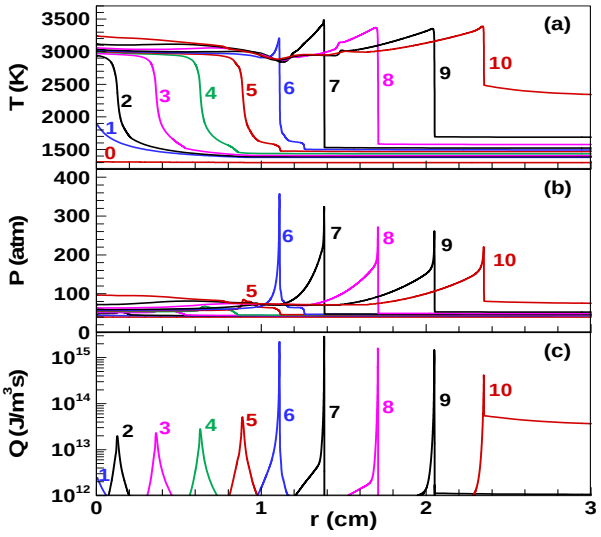

Fig. 4 Temporal evolution of the (a) temperature (b) pressure and (c) heat release rate distributions during the autoignitive reaction front propagation in a stoichiometric CH_4/air mixture with a hot spot of r_0 = 9 mm and ξ = 2.8. The time sequence for lines #0~10 is 0: 0 μs, 1: 285.5 μs, 2: 288.4 μs, 3: 293.4 μs, 4: 296.4 μs, 5: 299.7 μs, 6: 301.4 μs, 7: 302.8 μs, 8: 304.6 μs, 9: 306.5 μs, 10: 308.2 μs.

Figure 5 shows the detonation development regime obtained from 1D simulations using the reduced GRI mechanism. It also plots the maximum pressure for 96 sets of (ξ, ε) considered in simulations. The criteria for detonation development is that the reaction front speed is above 90% of the C-J detonation speed (i.e., $u_a > 0.9V_{CJ}$ = 1653 m/s) and the maximum pressure is above two times of the equilibrium pressure (i.e., $P_{max} > 2P_e$ = 200 atm). The detonation development was shown to occur for $\xi_l < \xi < \xi_u$, i.e., in the regime on the right side of the C-shaped curve in Fig. 4. At small ξ below the lower branch of the C-shaped curve (i.e., $\xi < \xi_l$), supersonic autoignitive reaction front occurs; while at large ξ above the upper branch (i.e., $\xi > \xi_u$), subsonic reaction front appears. Figure 5 shows that near the lower branch of the C-shaped curve, the maximum pressure changes abruptly. However, around the upper branch of the C-shaped curve, the maximum pressure varies further more smoothly with ξ, compared with that of the lower branch in Fig. 5. The maximum pressure is about 200 to 210 atm in the proximity of the upper branch, which is close to

the pressure criterion of detonation peninsula. Consequently, as Fig. 6 (a) shows, reduced GRI mechanism inclines to show a much steeper upper branch than other two mechanisms, especially in the criterion of 200 atm. It is noted that the present detonation regime is much broader than the one reported by Pan et al.[22] for methane/air. This may because stronger criterion for detonation development was used by Pan et al.[22]

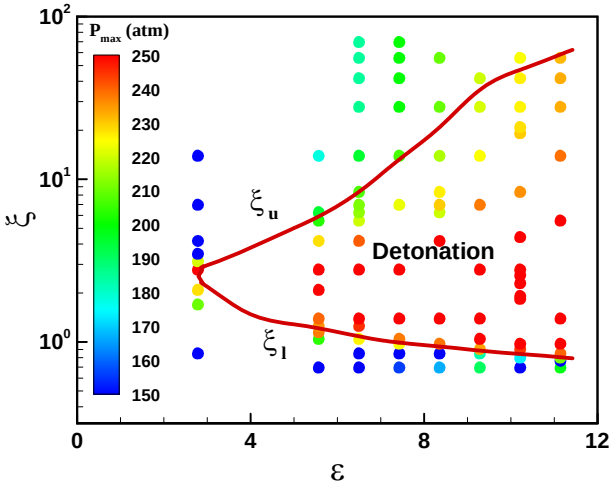

Fig. 5 Maximum pressure and detonation regime predicted by the reduced GRI mechanism for a stoichiometric CH_4/air mixture initially at $T_0 = 1300$ K and $P_0 = 40$ atm.

Figure 6 compares the detonation development regimes predicted by three kinetic models: GRI reduced, Aramco 3.0, and FFCM-1. Qualitatively, all these kinetic models predict the C-shaped boundaries for the detonation development regime. However, quantitatively, there are notable discrepancies among the upper and lower boundaries predicted by different kinetic models. For example, the upper branch of the C-shaped curve predicted by the reduced GRI mechanism is much higher than those by FFCM-1 and Aramco 3.0. Recent experimental data on the ignition delay time (see Figs. 6 and 16 in work of Karimi et al. [53]) and the laminar flame speed (see Fig. 10 in work of Movaghar et al. [54] and Fig. 6 in work of Wang et al. [55]) indicate that FFCM-1 can be used for methane oxidation at high pressures. Therefore, FFCM-1 is recommended for the calculation of detonation development from a hot spot and the detonation development regime. It is noted that

currently there are still no experimental data which can be used to validate the kinetic model FFCM-1 in terms of predicting flame propagation around the speed of sound jest before detonation initiation.

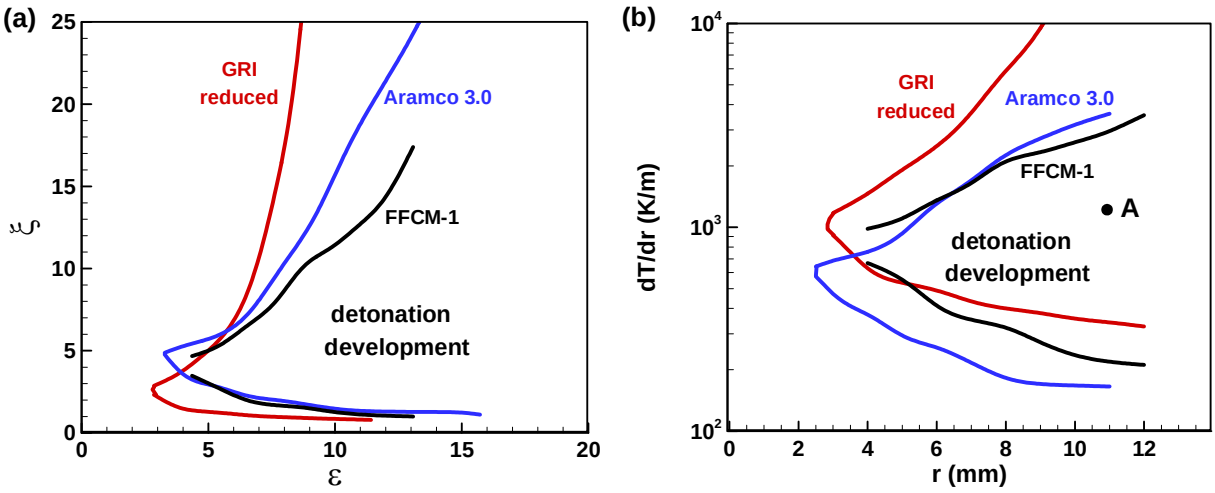

Fig. 6 Detonation development regimes predicted by different kinetic models for a stoichiometric CH_4/air mixture initially at T_0 = 1300 K and P_0 = 40 atm in the plots of (a) ξ–ε and (b) dT/dr-r. Point A corresponds to $(dT/dr)_0$ = -1050 K/m and = 11 mm.

The detonation development process from the same hot spot but predicted by different kinetic models is shown in Fig. 7. Figure 7(a) shows that the reduced GRI mechanism predicts a very strong detonation initiation with a peak pressure close to 600 atm. For Aramco 3.0 and FFCM-1, the peak pressures are both below 300 atm. Therefore, the knock intensities predicted by different kinetic models have great difference. Moreover, different features after detonation propagation were predicted by different kinetic models. A typical homogeneous explosion was predicted by the reduced GRI. For Aramco 3.0, the leading shock decouples with the supersonic reaction front due to the temperature gradient ahead of the original detonation front. The supersonic reaction front consumes the remaining unburnt gas and causes a smooth rise of temperature. The FFCM-1 model predicts a combination of the former two features. In addition, the corresponding values of ξ for

reduced GRI, FFCM-1 and Aramco 3.0 are 2.56, 5.06, 8.07 respectively. Figure 7(d) shows that the duration of detonation propagation is different: longest by the reduced GRI mechanism and shortest by Aramco 3.0, decreasing as ξ increases from 2.56 to 8.07. Besides, there is notable difference in the reaction front propagation speeds before the detonation development: around 250 m/s, 450 m/s and 700 m/s for Aramco 3.0, FFCM-1 and reduced GRI mechanisms, respectively. It is difficult to experimentally reproduce the detonation initiation from a hot spot predicted by the simulations and to measure these reaction front propagation speeds. Therefore, the detonation development regime cannot be directly validated by experiments. The kinetic models need to validated by the ignition delay time measured in shock tubes [53] and the laminar flame speeds measured from expanding spherical flames [50] under engine-relevant conditions.

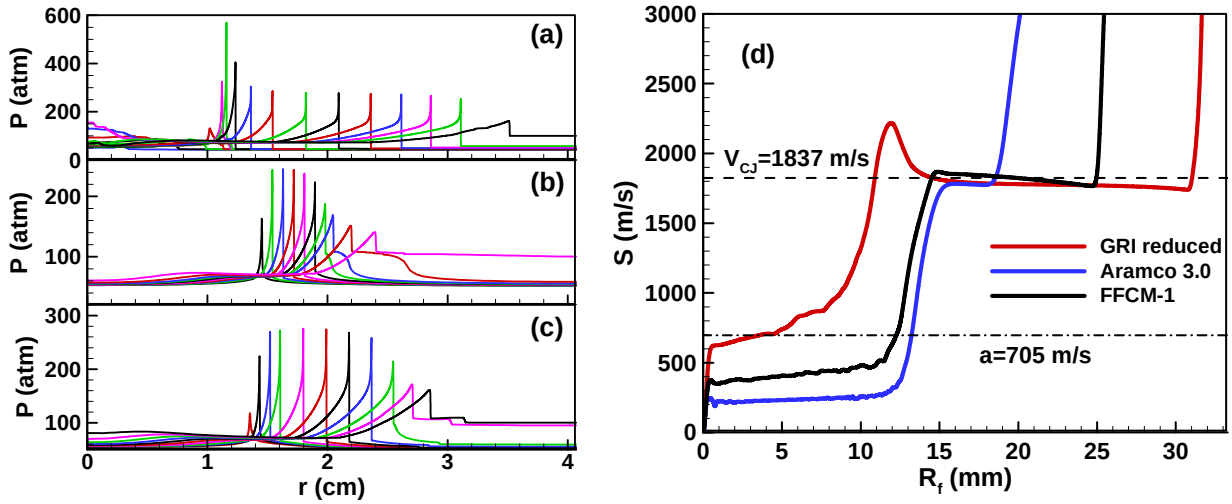

Fig. 7 Temporal evolution of the pressure distributions during the autoignitive reaction front propagation from a hot spot with $(dT/dr)_0 = -1050$ K/m and $r_0 = 11$ mm (corresponding point A in Fig. 6(b)) predicted by different kinetic models: (a) GRI reduced, (b) Aramco 3.0, and (c) FFCM-1. Figure (d) shows the reaction front propagation speed S as a function of its location R_f. The CJ detonation speed (V_{CJ} = 1837 m/s) and sound speed (a = 705 m/s) are denoted by the horizontal dashed and dash-dotted lines, respectively.

Theoretically, $\xi = 1$ would be the condition with the strongest detonation development, for it represents the reaction front moving in the identical speed with the shock. Nevertheless, numerical simulation tends to require a larger ξ. By varying $(dT/dr)_0$ (or ξ) when each r_0 (or ε) is fixed, we find that reduced GRI has its maximum P_{max} when ξ varies from 2 to 3. However, FFCM-1 and Aramco mechanism show ranges of 3~5. When r_0 (or ε) is set, as $(dT/dr)_0$ (or ξ) deviate more from the condition with the maximum P_{max}, detonation seems to be weakened. If $(dT/dr)_0$ (or ξ) is rising from the condition with the maximum P_{max}, detonation inclines to end with the decouple of shock and supersonic reaction front, which is particularly explicit in Aramco.

Finally, in Fig. 8 we compared the detonation regimes of different fuels including syngas[11] methane (this work), and dimethyl ether (DME)[56], n-heptane[56], toluene reference fuel (42.8% isooctane, 13.7% n-heptane, 43.5% toluene)[20]. Notable difference is observed among the detonation regimes of these fuels, indicating that the detonation development regime strongly depends on fuel. Therefore, the detonation peninsular for syngas cannot be used for other fuels. It is noted that different kinetic models were used to calculate the detonation development regimes for different fuels: the kinetic model extracted from GRI-Mech 2.11 by Gu et al. [11] for syngas, the kinetic model of Burke et al. [57] for DME, the kinetic model of Liu et al. [58] for n-heptane, and the LLNL kinetic model[59] for toluene reference fuel. Since the degree of variation among the lines of Nos. 5-7 is shown to be smaller than that of lines of Nos. 1-4, the influence of the kinetic model on the calculation of detonation development regime is weaker than that of the fuel type. Since both fuel type and kinetic model affects the detonation development regime, it is impossible to distinguish between the effects of the different kinetic models and the effects of the different fuels. Furthermore, the detonation development regime also depends on the thermal conditions (temperature and pressure) and composition (equivalence ratio, blending of exhausted gas) of the reactants.[20] This

further complicates the detonation regime and deserves and needs to be explored in future studies.

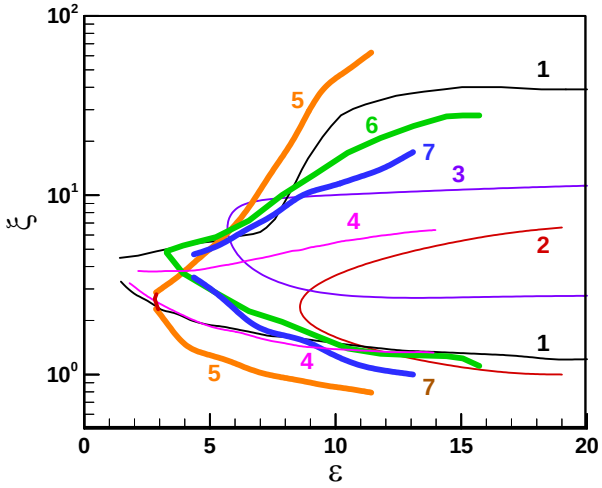

Fig. 8 The detonation regime in the ξ-ε diagram for different stoichiometric fuel/air mixtures: line #1 for H_2/CO/air at $T_0 = 1000$ K and $P_0 = 50$ atm[11], #2 for DME/air at $T_0 = 1035$ K and $P_0 = 40$ atm[56], #3 for n-heptane/air at $T_0 = 802$ K and $P_0 = 40$ atm[56], #4 for toluene reference fuel (42.8% isooctane, 13.7% n-heptane, 43.5% toluene at $T_0 = 1000$ K and $P_0 = 50$ bar[20]; and # 5, #6, #7 for CH_4/air at $T_0 = 1300$ K and $P_0 = 40$ atm, respectively from reduced GRI mechanism, Aramco 3.0 mechanism and FFCM -1 mechanism (this work).

4. Conclusions

Numerical simulations were conducted to investigate the autoignitive reaction front propagation and detonation development from a hot spot in stoichiometric methane/air mixtures. The performance of different kinetic models for methane oxidation was examined. First, the ignition delay time, excitation time, critical temperature gradient, thermal sensitivity and reduced activation energy were calculated using eight kinetic models for methane. Comparison among these results indicates that there are notable discrepancies among the predictions by different kinetic models. Therefore, it was expected that different detonation development regime may be predicted by different kinetic models for the same hot spot and initial conditions. Then, the detonation development regimes were obtained from 1D simulations using three kinetic models, the reduced

GRI 3.0 Mech., Aramco 3.0 and FFCM-1. Qualitatively, all these kinetic models predict the C-shaped boundaries for the detonation development regime. However, quantitatively, there are notable discrepancies among the upper boundary and the upper branch of the C-shaped curve predicted by the reduced GRI mechanism is much higher than those by FFCM-1 and Aramco 3.0. Furthermore, comparison among the results obtained for different fuels demonstrates that the detonation development regime is fuel-dependent and thereby the detonation peninsula for syngas reported by Bradley and coworkers might not work for all fuels.

The present results indicate that further efforts need to be devoted to the development and validation of the kinetic model for methane at engine-relevant conditions. Unfortunately, it is difficult to validate the detonation development regimes directly through experiments. The kinetic models need to be further validated against the ignition delay time measured in shock tubes and the laminar flame speeds measured from expanding spherical flames under engine-relevant conditions[48]. Besides, the detonation development regimes at different initial pressures, temperatures, equivalence ratios and exhaust gas recirculation addition need to be explored in future studies. The present results indicate the limitation of the detonation development regime using the two well-known non-dimensional parameters introduced by Bradley and coworkers[11]. Therefore, further efforts need to be devoted to the exploration of new parameters for a universal prediction of the detonation development regimes.

Acknowledgments

This work was supported by National Natural Science Foundation of China (Nos. 91741126 and 51861135309).

References

1. Korakianitis T, Namasivayam AM and Crookes RJ. Natural-gas fueled spark-ignition (SI) and compression-ignition (CI) engine performance and emissions. *Prog Energy Combust Sci* 2011; 37: 89-112.

2. Zhen X, Wang Y, Xu S, Xu S, Zhu Y, Tao C, Xu C and Song M. The engine knock analysis – an overview. *Appl Energy* 2012; 92: 628-636.

3. Dahnz C and Spicher U. Irregular combustion in supercharged spark ignition engines–pre-ignition and other phenomena. *Int J Engine Res* 2010; 11: 485-498.

4. Kalghatgi G. Developments in internal combustion engines and implications for combustion science and future transport fuels. *P Combust Inst* 2015; 35: 101-115.

5. Kalghatgi G. Knock onset, knock intensity, superknock and preignition in spark ignition engines. *Int J Engine Res* 2018; 19: 7-20.

6. Kalghatgi GT and Bradley D. Pre-ignition and 'super-knock' in turbo-charged spark-ignition engines. *Int J Engine Res* 2012; 13: 399-414.

7. Wang Z, Liu H and Reitz RD. Knocking combustion in spark-ignition engines. *Prog Energy Combust Sci* 2017; 61: 78-112.

8. Wang Z, Liu H, Song T, Song T, Qi Y, He X, Shuai S and Wang J. Relationship between super-knock and pre-ignition. *Int J Engine Res* 2015; 16: 166-180.

9. Wang Z, Qi Y, He X, Wang J, Shuai S and Law CK. Analysis of pre-ignition to super-knock: hot spot-induced deflagration to detonation. *Fuel* 2015; 144: 222-227.

10. Bates L, Bradley D, Paczko G and Peters N. Engine hot spots: modes of auto-ignition and reaction propagation. *Combust Flame* 2016; 166: 80-85.

11. Gu XJ, Emerson DR and Bradley D. Modes of reaction front propagation from hot spots. *Combust Flame* 2003; 133: 63-74.

12. Kapila A, Schwendeman D, Quirk J and Hawa J. Mechanisms of detonation formation due to a temperature gradient. *Combust Theory Modell* 2002; 6: 553-594.

13. Sharpe GJ and Short M. Detonation ignition from a temperature gradient for a two-step chain-branching kinetics model. *J Fluid Mech* 2003; 476: 267-292.

14. Bates L and Bradley D. Deflagrative, auto-ignitive, and detonative propagation regimes in engines. *Combust Flame* 2017; 175: 118-122.

15. Bradley D and Kalghatgi GT. Influence of autoignition delay time characteristics of different

fuels on pressure waves and knock in reciprocating engines. *Combust Flame* 2009; 156: 2307-2318.

16. Rudloff J, Zaccardi J-M, Richard S and Anderlohr J. Analysis of pre-ignition in highly charged SI engines: Emphasis on the auto-ignition mode. *P Combust Inst* 2013; 34: 2959-2967.

17. Dai P, Qi C and Chen Z. Effects of initial temperature on autoignition and detonation development in dimethyl ether/air mixtures with temperature gradient. *P Combust Inst* 2017; 36: 3643-3650.

18. Robert A, Richard S, Colin O and Poinsot T. LES study of deflagration to detonation mechanisms in a downsized spark ignition engine. *Combust Flame* 2015; 162: 2788-2807.

19. Robert A, Zaccardi J-M, Dul C, Guerouani A and Rudloff J. Numerical study of auto-ignition propagation modes in toluene reference fuel–air mixtures: toward a better understanding of abnormal combustion in spark-ignition engines. *Int J Engine Res* 2018; 00: 1-12.

20. Guerouani A, Robert A and Zaccardi J-M. Detonation peninsula for TRF-air mixtures: assessment for the analysis of auto-ignition events in spark-ignition engines. SAE Technical Paper 2018-01-7191, 2018.

21. Dai P, Chen Zand Gan X. Autoignition and detonation development induced by a hot spot in fuel-lean and CO2 diluted n-heptane/air mixtures. *Combust Flame* 2019; 201: 208-214.

22. Pan J, Dong S, Wei H, Li T, Shu G and Zhou L. Temperature gradient induced detonation development inside and outside a hotspot for different fuels. *Combust Flame* 2019; 205: 269-277.

23. Qi C, Dai P, Yu H and Chen Z. Different modes of reaction front propagation in n-heptane/air mixture with concentration non-uniformity. *P Combust Inst* 2017; 36: 3633-3641.

24. Zhang T, Sun W and Ju Y. Multi-scale modeling of detonation formation with concentration and temperature gradients in n-heptane/air mixtures. *P Combust Inst* 2017; 36: 1539-1547.

25. Dai P and Chen Z. Effects of NOx addition on autoignition and detonation development in DME/air under engine-relevant conditions. *P Combust Inst* 2019; 37: 4813-4820.

26. Bates L, Bradley D, Gorbatenko I and Tomlin A. Computation of methane/air ignition delay and excitation times, using comprehensive and reduced chemical mechanisms and their relevance in engine autoignition. *Combust Flame* 2017; 185: 105-116.

27. Zeldovich YB. Regime classification of an exothermic reaction with nonuniform initial conditions. *Combust Flame* 1980; 39: 211-214.

28. Lee J, Knystautas R and Yoshikawa N. Photochemical initiation of gaseous detonations. *Acta Astronaut.*1980; 5(11-12): 971-982.

29. Pan J, Shu G and Wei H. Interaction of flame propagation and pressure waves during knocking combustion in spark-ignition engines. *Combust Sci Technol* 2014; 186: 192-209.

30. Gao Y, Dai P and Chen Z. Numerical studies on autoignition and detonation development from a hot spot in hydrogen/air mixtures. *Combust Theory Modell*. 2019; 24: 245-261..

31. Dai P, Chen Z, Chen S and Ju Y. Numerical experiments on reaction front propagation in n-heptane/air mixture with temperature gradient. *P Combust Inst* 2015; 35: 3045-3052.

32. Zhang T, Sun W, Wang L and Ju Y. Effects of low-temperature chemistry and turbulent transport on knocking formation for stratified dimethyl ether/air mixtures. *Combust Flame* 2019; 200: 342-353.

33. Wang C, Qian C, Liu J and Liberman M. Influence of chemical kinetics on detonation initiating by temperature gradients in methane/air. *Combust Flame* 2018; 197: 400-415.

34. Liberman M, Wang C, Qian C and Liu J. Influence of chemical kinetics on spontaneous waves and detonation initiation in highly reactive and low reactive mixtures. *Combust Theory Modell* 2019; 23: 467-495.

35. Chen Z, Burke MP and Ju Y. Effects of Lewis number and ignition energy on the determination of laminar flame speed using propagating spherical flames. *P Combust Inst* 2009; 32: 1253-1260.

36. Chen Zand Flame. Effects of radiation and compression on propagating spherical flames of methane/air mixtures near the lean flammability limit. *Combust Flame* 2010; 157: 2267-2276.

37. Dai P and Chen Z. Supersonic reaction front propagation initiated by a hot spot in n-heptane/air mixture with multistage ignition. *Combust Flame* 2015; 162: 4183-4193.

38. Qi C and Chen Z. Effects of temperature perturbation on direct detonation initiation. *P Combust Inst* 2017; 36: 2743-2751.

39. Yu H, Qi C and Chen Z. Effects of flame propagation speed and chamber size on end-gas autoignition. *P Combust Inst* 2017; 36: 3533-3541.

40. Zhang W, Faqih M, Gou X and Chen Z. Numerical study on the transient evolution of a premixed cool flame. *Combust Flame* 2018; 187: 129-136.

41. Li Z, Gou X and Chen Z. Effects of hydrogen addition on non-premixed ignition of iso-octane by hot air in a diffusion layer. *Combust Flame* 2019; 199: 292-300.

42. Mahdi F, Li H, Gou X and Chen Z. On laminar premixed flame propagating into autoigniting mixtures under engine-relevant conditions. *P Combust Inst* 2019; 37: 4673-4680.

43. Huang C, Qi C and Chen Z. Non-uniform ignition behind a reflected shock and its influence on

ignition delay measured in a shock tube. *Shock Waves* 2019; 29: 957-967.

44. Smith G, Tao Y and Wang H. Foundational fuel chemistry model version 1.0 (FFCM-1), http://nanoenergy.stanford.edu/ffcm1 (2016).

45. Chemical-Kinetic Mechanisms for Combustion Applications, http://web.eng.ucsd.edu/mae/groups/combustion/mechanism.html.

46. Zhou C, Li Y, Burke U, Banyon C, Somers K, Ding S and Khan S. An experimental and chemical kinetic modeling study of 1, 3-butadiene combustion: Ignition delay time and laminar flame speed measurements. *Combust Flame* 2018; 197: 423-438.

47. Gregory P, Golden D, Frenklach M, Moriarty N, Eiteneer B, Goldenberg M, Bowman T, Hanson R, Song S, Gardiner W, Lissianski V and Qin Z. GRI-Mech 3.0 (Tech. Rep.), http://www.me.berkeley.edu/gri_mech/.

48. Lu T and Law CK. A criterion based on computational singular perturbation for the identification of quasi steady state species: A reduced mechanism for methane oxidation with NO chemistry. *Combust Flame* 2008; 154: 761-774.

49. Hashemi H, Christensen JM, Gersen S, Levinsky H, Klippenstein S and Glarborg P. High-pressure oxidation of methane. *Combust Flame* 2016; 172: 349-364.

50. Zhao H, Fu J, Haas FM and Ju Y. Effect of prompt dissociation of formyl radical on 1, 3, 5-trioxane and CH_2O laminar flame speeds with CO_2 dilution at elevated pressure. *Combust Flame* 2017; 183: 253-260.

51. Shen X, Yang X, Santner J, Sun J and Ju Y. Experimental and kinetic studies of acetylene flames at elevated pressures. *P Combust Inst* 2015; 35: 721-728.

52. Wang H, You X, Joshi A, Davis SG, Laskin A, Egolfopoulos F and Law CK. High-temperature combustion reaction model of H_2/CO/C_1–C_4 compounds, http://www.ignis.usc.edu/USC_Mech_II.htm. (2007).

53. Karimi M, Ochs B, Liu Z, Ranjan D and Sun W. Measurement of methane autoignition delays in carbon dioxide and argon diluents at high pressure conditions. *Combust Flame* 2019; 204: 304-319.

54. Movaghar A, Lawson R and Egolfopoulos FN. Confined spherically expanding flame method for measuring laminar flame speeds: revisiting the assumptions and application to C_1-C_4 hydrocarbon flames. *Combust Flame* 2019; 212: 79-92.

55. Wang Y, Movaghar A, Wang Z, Liu Z, Sun W, Egolfopoulos FN and Chen Z. Laminar flame

speeds of methane/air mixtures at engine conditions: performance of different kinetic models and power-law correlations, *Combust and Flame*, 2020; 218: 101-108.

56. Dai P, Qi C and Chen Z. Effects of initial temperature on autoignition and detonation development in dimethyl ether/air mixtures with temperature gradient. *P Combust Inst* 2016; 36: 3643-3650.

57. Burke U, Somers KP, O'Toole P, Zinner CM, Marquet N, Bourque G, Pertersen EL, Metcalfe WK, Serinyel Z and Curran HJ. An ignition delay and kinetic modeling study of methane, dimethyl ether, and their mixtures at high pressures. *Combust Flame* 2015; 162: 315-330.

58. Liu S, Hewson JC, Chen JH and Pitsch H. Effects of strain rate on high-pressure nonpremixed n-heptane autoignition in counterflow. *Combust Flame* 2004; 137: 320-339.

59. Mehl M, Pitz WJ, Westbrook CK and Curran HJ. Kinetic modeling of gasoline surrogate components and mixtures under engine conditions. *P Combust Inst* 2011; 33: 193-200.